Gold Nanoparticle Incorporation into Porous Titania Networks Using an Agarose Gel Templating Technique for Photocatalytic Applications

Xingdong Wang,[†] David R. G. Mitchell,[‡] Kathryn Prince,[‡] Armand J. Atanacio,[‡] and Rachel A. Caruso*,[†]

PFPC, School of Chemistry, The University of Melbourne, Melbourne, Victoria 3010, Australia, and Australian Nuclear Science and Technology Organisation, PMB 1, Menai, NSW 2234, Australia

Received December 9, 2007. Revised Manuscript Received March 25, 2008

Porous titania networks containing gold nanoparticles have been synthesized and tested in photocatalytic applications. The porous structure was controlled using a templating technique, while a range of gold concentrations and a variety of routes were investigated to incorporate the gold nanoparticles. The influence of these parameters on the final structure (surface area and pore size), the gold crystal size, distribution, and content, and the photocatalytic activity of the porous materials were investigated. UV−vis diffuse reflectance spectra of the Au/TiO_2 materials showed strong absorbance at approximately 580 nm, indicating the successful incorporation of the gold species. X-ray diffraction analysis ascertained that the titania materials were crystalline (anatase phase) with gold peaks observed only when the gold content was greater than 0.25 wt %. Gold distribution and content in the materials were measured using secondary ion mass spectrometry and inductively coupled plasma mass spectrometry. From transmission electron microscopy analysis, the gold particle size and distribution varied with both the material preparation method and the concentration of gold used in the synthesis. Photocatalytic activity was dependent on the gold particle size and gold quantity. The highest photocatalytic activity under UV light irradiation as monitored by the photodecomposition of methylene blue was obtained for the Au/TiO_2 sample containing 2.0 wt % gold prepared by the deposition of gold onto prefabricated porous TiO_2.

Introduction

Contaminated water and polluted air have affected the environment and human health. Hence, much research has been undertaken to address this global issue. Ever since Fujishima and Honda discovered water photolysis in the presence of a titanium dioxide (TiO_2) electrode in 1972,[1] TiO_2-based semiconductor materials have been widely applied in environmental remediation because of the availability, low-cost, nontoxicity, stability, and efficiency of TiO_2. Differences in the three main crystal structures of TiO_2 (anatase, brookite, and rutile) result in each crystal having its own properties, which in turn leads to different applications for the various polymorphs. Anatase and rutile phases are commonly used in photocatalysis, with the anatase phase generally shows a higher photocatalytic activity.[2]

Anatase TiO_2 has a wide band gap of 3.2 eV, and therefore the anatase titania crystal can absorb light only with wavelengths less than ~380 nm.[3] Photocatalytic activity can be detrimentally affected by recombination of the electron and hole pairs produced upon photon absorption. Hence, the ability to either change the band gap of titania to allow photoactivity on irradiation with visible light or decrease the electron/hole recombination is being pursued.[4] The deposition of noble metals such as Au, Pt, Ru, Rh, Pd, and Ag onto TiO_2 surfaces is a very dynamic research area in terms of improving the photocatalytic activity of TiO_2.[5–13] Electron transfer from TiO_2 to metal nanoparticles can occur, thereby decreasing the number of electron/hole recombination events.

When Au/TiO_2 materials are applied in photocatalysis, the material preparation method plays an important role in determining the photocatalytic activity of the materials. The particle size and distribution of the gold and the gold−metal oxide interface are noticeably dependent on a range of conditions (such as metal concentration, solution pH, temperature of synthesis, aging time and temperature, and sample heating).[14,15] A variety of synthesis approaches have been

* Corresponding author. E-mail: rcaruso@unimelb.edu.au.
[†] The University of Melbourne.
[‡] Australian Nuclear Science and Technology Organisation.

(1) Fujishima, A.; Honda, K. *Nature* **1972**, *238*, 37.
(2) Linsebigler, A. L.; Lu, G. Q.; Yates, J. T. *Chem. Rev.* **1995**, *95*, 735.
(3) Wold, A. *Chem. Mater.* **1993**, *5*, 280.
(4) Hoffmann, M. R.; Martin, S. T.; Choi, W. Y.; Bahnemann, D. W. *Chem. Rev.* **1995**, *95*, 69.
(5) Sakthivel, S.; Shankar, M. V.; Palanichamy, M.; Arabindoo, B.; Bahnemann, D. W.; Murugesan, V. *Water Res.* **2004**, *38*, 3001.
(6) Jakob, M.; Levanon, H.; Kamat, P. V. *Nano Lett.* **2003**, *3*, 353.
(7) Dawson, A.; Kamat, P. V. *J. Phys. Chem. B* **2001**, *105*, 960.
(8) Kubo, W.; Tatsuma, T. *J. Mater. Chem.* **2005**, *15*, 3104.
(9) Iliev, V.; Tomova, D.; Bilyarska, L.; Eliyas, A.; Petrov, L. *Appl. Catal., B* **2006**, *63*, 266.
(10) Seery, M. K.; George, R.; Floris, P.; Pillai, S. C. *J. Photochem. Photobiol., A* **2007**, *189*, 258.
(11) Naito, S. *J. Chem. Soc., Chem. Commun.* **1985**, 1211.
(12) Solymosi, F.; Tombacz, I. *Catal. Lett.* **1994**, *27*, 61.
(13) Munuera, G.; Gonzalez-Elipe, A. R.; Espinos, J. P.; Navio, A. *J. Mol. Struct.* **1986**, *143*, 227.
(14) Bamwenda, G. R.; Tsubota, S.; Kobayashi, T.; Haruta, M. *J. Photochem. Photobiol., A* **1994**, *77*, 59.
(15) Wolf, A.; Schuth, F. *Appl. Catal., A* **2002**, *226*, 1.

10.1021/cm703509f CCC: $40.75
Published on Web 05/20/2008

investigated to prepare gold/titania materials, including deposition−precipitation,[16] coprecipitation,[17] ionized cluster beam deposition,[18] sputtering,[19] chemical vapor deposition,[20] sol−gel routes,[21] and combined radio frequency sputtering/sol−gel approach.[22]

The porosity of the photocatalyst material, accessibility to the reaction surface, and overall ease of use of the catalyst are also important factors. Photocatalytic efficiencies of TiO_2 are expected to be enhanced by the combination of controlled porosity and the addition of metal sites. Porosity enhances diffusion of the pollutant throughout the channels in the photocatalyst, and the metal particles act as electron sinks, which decrease the recombination of photon-produced electron/hole pairs within the TiO_2. Templating techniques provide control over both the internal (porosity and pore size) and the external (morphology and size) material properties.[23–26] Recently, Caruso et al. employed the porous structure of agarose gels as a template for the fabrication of porous inorganic oxides.[27] Sol−gel chemistry was conducted within the agarose gel. On removal of the agarose by heating, well-crystallized porous metal oxide structures were prepared. In this article, we describe the combination of the templating techniques with metal synthesis routes to obtain gold-modified porous titania nanocomposites that show enhanced photocatalytic activity.

It should also be mentioned that supported gold nanoparticles have received much attention because of the catalytic properties of the gold; for example, in the oxidation of CO at low temperature.[28–32] The size of the gold particles and the interaction of the gold with the catalyst support were crucial parameters to achieving active gold catalysts.[33–36] Typically, gold particle diameters were less than 5 nm and a common support was titania.[36] Therefore, although the focus in this article is photocatalysis, the materials synthesized in this research could also be potentially applied as supported catalysts.

(16) Haruta, M.; Tsubota, S.; Kobayashi, T.; Kageyama, H.; Genet, M. J.; Delmon, B. *J. Catal.* **1993**, *144*, 175.
(17) Haruta, M.; Yamada, N.; Kobayashi, T.; Iijima, S. *J. Catal.* **1989**, *115*, 301.
(18) Takaoka, G. H.; Hamano, T.; Fukushima, K.; Matsuo, J.; Yamada, I. *Nucl. Instrum. Methods Phys. Res., Sect. B* **1997**, *121*, 503.
(19) Sasaki, T.; Koshizaki, N.; Koinuma, M.; Matsumoto, Y. *Nanostruct. Mater.* **1999**, *12*, 511.
(20) Okumura, M.; Nakamura, S.; Tsubota, S.; Nakamura, T.; Azuma, M.; Haruta, M. *Catal. Lett.* **1998**, *51*, 53.
(21) Epifani, M.; Giannini, C.; Tapfer, L.; Vasanelli, L. *J. Am. Ceram. Soc.* **2000**, *83*, 2385.
(22) Armelao, L.; Barreca, D.; Bottaro, G.; Gasparotto, A.; Tondello, E.; Ferroni, M.; Polizzi, S. *Chem. Mater.* **2004**, *16*, 3331.
(23) Polarz, S.; Antonietti, M. *Chem. Commun.* **2002**, 2593.
(24) Caruso, R. A. *Top. Curr. Chem.* **2003**, *226*, 91.
(25) Davis, S. A.; Breulmann, M.; Rhodes, K. H.; Zhang, B.; Mann, S. *Chem. Mater.* **2001**, *13*, 3218.
(26) Caruso, R. A.; Antonietti, M. *Chem. Mater.* **2001**, *13*, 3272.
(27) Zhou, J. F.; Zhou, M. F.; Caruso, R. A. *Langmuir* **2006**, *22*, 3332.
(28) Cunningham, D. A. H.; Vogel, W.; Sanchez, R. M. T.; Tanaka, K.; Haruta, M. *J. Catal.* **1999**, *183*, 24.
(29) Solsona, B.; Conte, M.; Cong, Y.; Carley, A.; Hutchings, G. *Chem. Commun.* **2005**, 2351.
(30) Schumacher, B.; Plzak, V.; Kinne, M.; Behm, R. J. *Catal. Lett.* **2003**, *89*, 109.
(31) Li, W. C.; Comotti, M.; Schüth, F. *J. Catal.* **2006**, *237*, 190.
(32) Grunwaldt, J. D.; Kiener, C.; Wögerbauer, C.; Baiker, A. *J. Catal.* **1999**, *181*, 223.
(33) Wang, C. Y.; Liu, C. P.; Chen, J.; Shen, T. *J. Colloid Interface Sci.* **1997**, *191*, 464.
(34) Chen, M. S.; Goodman, D. W. *Catal. Today* **2006**, *111*, 22.
(35) Min, B. K.; Wallace, W. T.; Goodman, D. W. *Surf. Sci.* **2006**, *600*, L7.
(36) Haruta, M. *Catal. Today* **1997**, *36*, 153.

Experimental Section

Materials. The structured porous organic gel template was prepared using an agarose powder (molecular biology grade) from Scientifix. The metal alkoxide, titanium(IV) isopropoxide (97%) and gold salt, hydrogen tetrachloroauric acid, were obtained from Sigma-Aldrich. The solvents 2-propanol (99.5%) and ethanol (99.9%) were purchased from Univar. Methylene blue was from BDH Chemical Ltd. The water used in all experiments was filtered through a Millipore Milli-Q purification system and had a resistivity higher than 18.2 MΩ cm.

Preparation of Agarose and Au/Agarose Gel Template. Agarose gel: Agarose powder (2 g) was added slowly to a beaker containing water (98 mL) at room temperature, with vigorous stirring to create a cloudy suspension. The suspension was heated until boiling for 5−10 min, forming a clear solution. It was then immediately poured gently into molds (24 mm diameter × 150 mm pyrex test tubes) and sealed with Parafilm. The samples were left at room temperature overnight to allow for complete gelation. The gelled product was removed by inserting a thin spatula down the side of the tube to create an air bubble and then sliding the gelled agarose out.

Au/agarose gel: The aqueous agarose solutions were heated as above until the solutions became clear, and then hydrogen tetrachloroauric acid (0.25−2.5 mL of a 100 mM $HAuCl_4$ aqueous solution) was added. After briefly being stirred further, the samples were gelled following the procedure above.

Preparation of TiO_2 Porous Network as a Control. First, the as-synthesized agarose gels were cut into smaller pieces (0.5 × 0.5 × 0.5 cm^3) and transferred from water into ethanol in three steps (water-to-ethanol volume ratio 2:1, 1:2, then 0:1, soaking 6 h in each solution), and similarly from ethanol to 2-propanol. Subsequently, the gel pieces (6 g) were soaked in 70 wt % titanium(IV) isopropoxide in 2-propanol solution (22 mL) for 18 h, before being transferred into a water/2-propanol (1:1 v/v, 22 mL) solution for hydrolysis and condensation reactions (6 h). The samples were then removed from solution and dried at room temperature for 2 days followed by 6 h at 60 °C. To remove the agarose template and crystallize the inorganic oxide, the samples were heated at 450 °C (heating rate 3.54 °C min^{-1}) under flowing air for 10 h.

Preparation of Au/TiO_2 Nanocomposites (Routes I to V). The method to incorporate gold nanoparticles into the TiO_2 structure varied across the synthesis routes labeled I to V, shown schematically in Scheme 1. In all cases, the gold was added in the dark. In route I, the gold was incorporated during the agarose gelation stage as described above, resulting in a Au/agarose gel. This gel was then used for titania precursor infiltration following the same procedure as described above for the control TiO_2 sample. In route II, the preformed agarose gel template (40 g) was cut into smaller pieces (0.5 × 0.5 × 0.3 cm^3) and then soaked in a gold salt solution (0.25 mM $HAuCl_4$ aqueous solution, 100 mL) for 15 days. These samples were not treated further because of inhomogeneous gold distribution as will be discussed in the Results and Discussion. In route III, before infiltrating with the titanium isopropoxide, gold salt solutions (volumes of 0.125−2.5 mL of a 100 mM $HAuCl_4$ in 2-propanol) were added to the 70 wt % titanium precursor in 2-propanol solution, making a total volume of 22 mL. After the solution was shaken to obtain a homogeneous solution, the agarose gel was added for precursor infiltration. The samples underwent

Scheme 1. Schematic Representation Indicating the Steps during Synthesis When the Gold Salt May Be Added for the Preparation of Porous Au/TiO_2 Materials

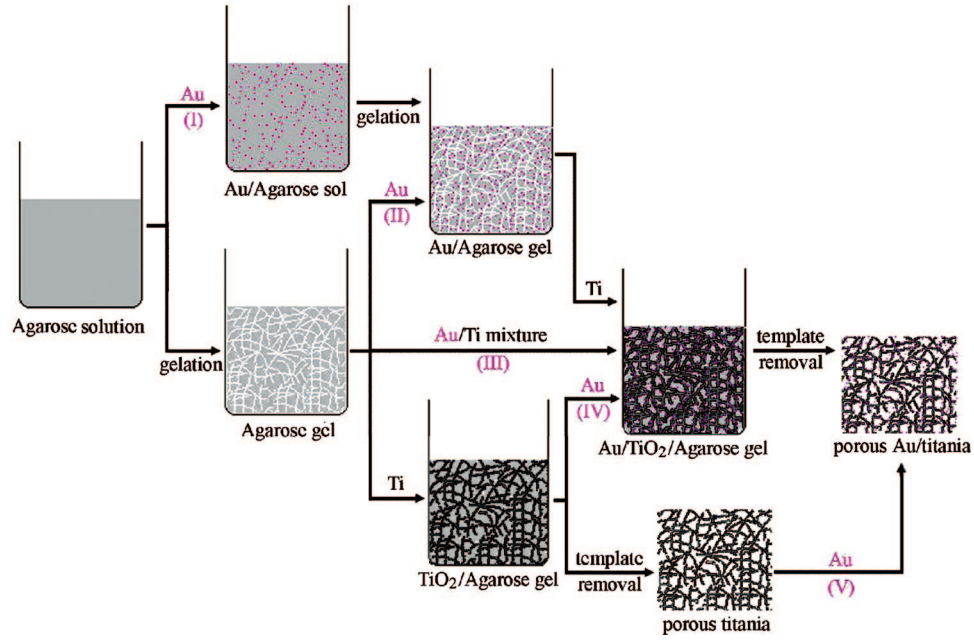

hydrolysis/condensation, drying and heating as described above for the control TiO_2 sample. In route IV, the 22 mL hydrolysis solution, 2-propanol/water (1:1 v/v), contained various volumes of gold salt solution (0.125−2.5 mL 100 mM $HAuCl_4$ aqueous gold stock solution). The titanium alkoxide infiltrated agarose pieces were placed into this solution to undergo hydrolysis and condensation reactions, with drying and calcination proceeding as for the TiO_2 control. In route V, with slight modification of the conventional deposition−precipitation (DP) method,[16] the calcined anatase TiO_2 porous structures (1 g) were immersed in a series of 15 mL aqueous solutions containing 0.125−2 mL of 100 mM $HAuCl_4$ solution at pH 7, overnight at room temperature. The solutions were then heated at 70 °C for 3 h to deposit $Au(OH)_3$ on the surfaces (both internal and external) of the TiO_2 porous structure. The composites were washed with Milli-Q water three times, vacuum-dried in a desiccator overnight, and finally calcined under flowing air at 300 °C for 5 h. Consistent temperature and drying conditions are crucial to reproduce samples with the same gold particle size and content.

Characterization. Scanning electron microscopy (SEM, Philips XL30 or FEI QUANTA 200F, operated at 20 kV) was used to examine the morphology of the samples. To prepare the as-synthesized agarose gel or Au/agarose gel samples for SEM, they were solvent-exchanged from water into ethanol and then into acetone before being dried using a carbon dioxide critical point drying technique (Baltec CPD 030 critical point dryer). The calcined samples were broken into several pieces so that fresh surfaces could be viewed. The samples were mounted onto carbon-coated SEM stubs and then sputter-coated with gold using an Edwards S150B gold sputter coater.

Transmission electron microscopy (TEM) images were taken using either a Philips CM120 BioTWIN TEM operating at 120 kV or a JEOL 2010F TEM operating at 200 kV, fitted with a Gatan imaging filter and an Oxford Instruments ISIS energy dispersive X-ray spectroscopy system for qualitative analysis. The samples were embedded in an LR-white resin and ultramicrotomed to a thickness of 90 nm before TEM analysis.

Nitrogen gas sorption measurements were conducted on a Micromeritics 3000 Tristar surface area and porosity analyzer at 77 K. Samples were evacuated at 60 °C (organic-containing samples) or 150 °C (inorganic samples) overnight before analysis. Surface areas were calculated by using the Brunauer−Emmett−Teller method. X-ray diffraction (XRD) was performed using a Philips PW1800 diffractometer (Cu Kα radiation wavelength of 1.54045 Å) to characterize the crystal phase and size of the final product.

UV−vis absorbance spectra of the gold sols were obtained using a CARY50 Bio UV−visible spectrophotometer, while UV−vis diffuse reflecting spectra of Au/TiO_2 composites were recorded on a Cary 5G UV−vis IR spectrophotometer.

Thermogravimetric analysis (TGA) and differential thermal analysis (DTA) were performed on a Mettler Toledo TGA/SDTA851e analyzer. The weight loss of organic and the amorphous to anatase phase transition temperature of the TiO_2 were studied by TGA and DTA. The samples were stabilized at 25 °C for 5 min before they were heated from 25 to 800 °C with a heating rate of 10 °C min^{-1}, under oxygen (30 mL min^{-1}).

The gold content in the composites was measured by inductively coupled plasma mass spectrometry (Varian ICP-MS). The calcined samples (5 mg) were dissolved in a HF (48%) + HNO_3 (69%) (1:1, v/v) solution in Teflon beakers at 110 °C for 2 h, and then the acid was evaporated at 130 °C before redissolving the solid overnight in aqua-regia. The samples were diluted by factors of 6 × 10^5 to 6 × 10^6 with 5% HCl spiked with cobalt and rhenium as internal standards. A calibration curve was obtained with a series of mixed gold (1.9 to 24 ng g^{-1}) and titanium (310 to 390 ng g^{-1}) standard solutions, allowing gold and titanium concentrations of the solution to be determined.

The distribution of the gold in the porous titania was investigated using a Camera IMS 5f dynamic secondary ion mass spectrometer (SIMS). The samples were mounted into EPO-THIN epoxy resin (Selby-Biolab) and polished carefully to achieve a smooth surface. The surface of the samples was sputter-coated with carbon to minimize charging during SIMS analysis. A 10 keV Cs^+ primary ion source was used to generate negative secondary ions (^{18}O, ^{49}Ti, $^{49}Ti^{18}O$, $^{49}Ti^{16}O$,$^{49}Ti^{16}O_2$, $^{49}Ti^{18}O_2$, ^{197}Au), which were counted for 1 s each per cycle on an ETP electron multiplier. A 60 nA primary ion beam, with an approximate diameter of ∼50 μm, was rastered over each sample surface, creating a crater with ap-

proximate dimensions of 250 × 250 μm^2. An aperture in the secondary column was used to provide an analytical area of diameter 55 μm in all measurements, thereby minimizing any crater edge effects in the analysis. Each sample surface was sputtered for around 1000 s before analysis to enable equilibrium sputtering conditions to be achieved. Further Cs^+ bombardment for 2000 s allowed stable counts for each mass channel of interest to be collected. The resulting craters were around 5-μm deep. Crater depth was determined using a KLA Tencor Alpha-step IQ stylus profilometer.

Photocatalysis. To study the photocatalytic activity of the samples, the photocatalyst (0.5 g L^{-1}) was added to 160 mL of aqueous methylene blue solution (50 mg L^{-1}) under continuous stirring and left overnight in the dark to equilibrate. The solution was placed into a water jacketed reaction chamber (at 20 ± 0.5 °C) and continuously bubbled with air for 30 min to stabilize the reactor solution. A 500 W Hg (Xe) globe (Oriel) with a dichroic mirror (66226, Oriel, 280 < λ < 400 nm) was used to pass light vertically through the quartz reactor lid. At regular irradiation time intervals (0, 10, 20, 30, 40, 50, and 60 min), aliquots of the solution were withdrawn and centrifuged (15000 rpm, 10 min). The supernatant of these solutions was used to monitor the change of methylene blue concentration via UV−vis absorbance spectroscopy.

Results and Discussion

Fabrication of the Au/TiO_2 Nanocomposite. Five routes were studied to synthesize porous Au/TiO_2 composites using the agarose gel template for structural control. The routes were differentiated according to the stage at which gold was added in the synthesis as illustrated in Scheme 1. The basic fabrication involved the following steps: (i) making the agarose gel template (by heating agarose in aqueous solution and then cooling to form the gel), (ii) solvent exchange to facilitate sol−gel method using the alkoxide precursor, (iii) titania precursor infiltration into the template, followed by (iv) hydrolysis and condensation reactions to achieve amorphous titania, and finally, (v) calcination to remove the agarose and crystallize the titania.

In route I, the gold salt was added during template formation. In route II, the gold salt was incorporated into the preformed agarose gel. In both routes I and II, the agarose template worked as both a reducing agent and an organic support, thereby forming and stabilizing the gold nanoparticles in the agarose gel structure.[37] In route III, the gold salt was added with the titanium dioxide precursor during template infiltration. In route IV, the gold was distributed throughout the structure during the hydrolysis and condensation step. In route V, gold was introduced to the crystallized titania structure using a modified DP method after the agarose template was removed. The key differences between the method used here and the conventional DP method are: (i) route V using porous networks instead of nonporous TiO_2, such as commercial P25 or TiO_2 synthesized by sol−gel method, (ii) the gold precursor concentration in route V was around six times higher than the conventional DP method, and (iii) the obtained gold deposition yield (∼90%), discussed later, was significantly higher than the average for the conventional DP method.[38]

Typically, in route I, the gold particles formed gradually, indicated by the agarose gel containing the gold nanoparticles changing color from slightly yellow to a distinct red, because of the plasmon resonance of the gold nanoparticles. Here, the agarose acted as the reducing agent, reducing the Au(III) to Au(0).[37] It was reported that the color of gold nanoparticles, which correlate to the surface plasmon band, was influenced by various parameters such as the particle size and shape, and the refractive index of the surrounding media.[39,40] The gold particles within the agarose gel gave absorbance peaks at approximately 550 nm (not shown), indicative of a gold particle size between 5 and 20 nm.[40]

In route II, an uneven distribution of the gold nanoparticles was found in the agarose gel: the gold accumulated in the center of the agarose gel piece with two layers of gold, lilac in color, evident when viewing the sample through the smallest (0.3 cm) edges. The UV−vis spectrum (not shown) of the aqueous gold precursor solution initially showed a gold salt peak at 288 nm and no plasmon absorbance. After the addition of agarose gel to this solution, the absorbance of the salt peak dropped by 50%, and a small absorbance band appeared at ∼570 nm. This plasmon peak increased slightly in intensity over the following 15 days. Thus, approximately half of the salt had been incorporated into the agarose, and the rest remained in solution. Because of the inhomogeneous distribution of gold nanoparticles in the agarose gel, samples from route II were not used to prepare Au/TiO_2 networks and were not further investigated.

The Au/agarose gel/amorphous TiO_2 samples were light purple (route I), light blue to blue (route III), and yellow (route IV) in color. The samples were calcined at 450 °C, removing the agarose template, crystallizing the titania, and resulting in gold nanoparticles being dispersed throughout the porous titanium dioxide structure. All the samples became blue in color after calcination. The mechanism by which the gold was reduced differed from route III to V. In route III, the gold was reduced during two different stages of the synthesis. The gold precursor remained yellow during the infiltration step and was reduced to gold nanoparticles during the hydrolysis step (visually observed by color change from yellow to blue), thus indicating that aqueous conditions were required for the reduction of the gold by either the agarose or alcohol present during hydrolysis. The second stage of reduction occurred during calcination. For route IV, the gold reduction only takes place during the calcination step. In route V (the DP process), the gold species in solution was transformed from $AuCl_4^-$ to $Au(OH)_nCl_{4-n}^-$ ($n = 1-3$)[36] and was then reduced to Au(0) during heating.

The mechanical stability of the inorganic structures was found to depend on the gold content, with mechanical strength decreasing with increasing gold content. Structure collapse was observed, indicated by the formation of a relatively dense and less porous material (e.g., Figure 1d), at gold contents of ⩾0.5 wt % for route I, and ⩾5 wt % for both routes III and IV. However, for route V the porous structure (fabricated before the addition of the gold salt) was maintained for gold contents as high as 16 wt %. The reason

(37) Wang, X. D.; Egan, C. E.; Zhou, M. F.; Prince, K.; Mitchell, D. R. G.; Caruso, R. A. *Chem. Commun.* **2007**, 3060.
(38) Zanella, R.; Delannoy, L.; Louis, C. *Appl. Catal., A* **2005**, *291*, 62.
(39) Underwood, S.; Mulvaney, P. *Langmuir* **1994**, *10*, 3427.
(40) Mulvaney, P. *Langmuir* **1996**, *12*, 788.

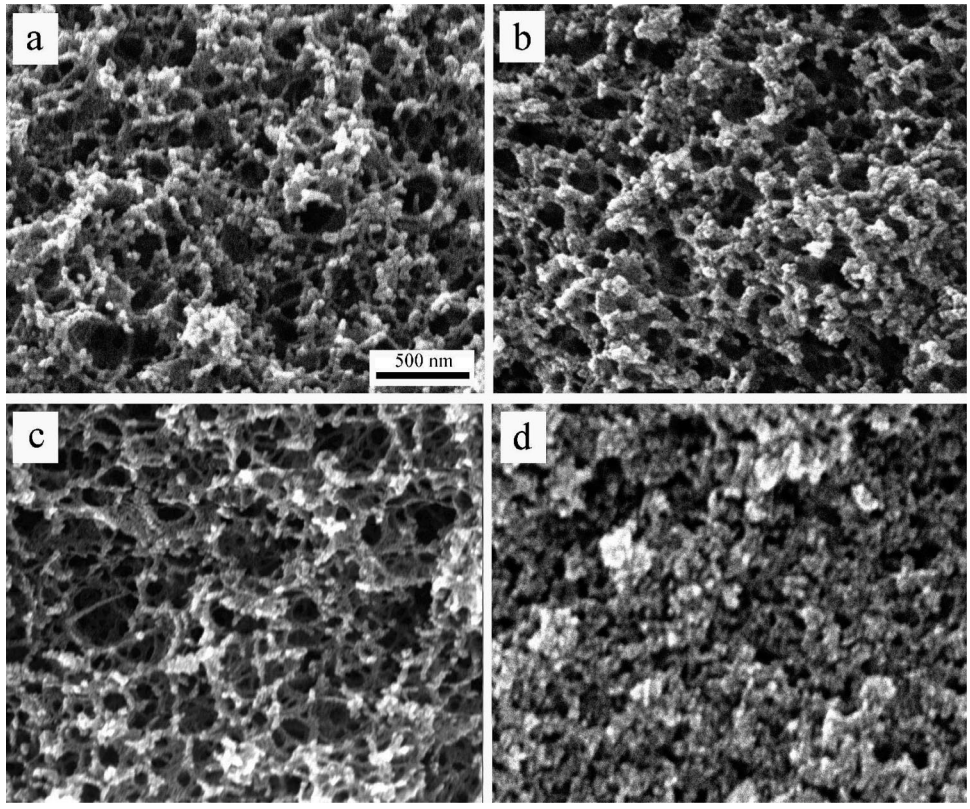

Figure 1. SEM images (all at the same scale) of the Au/TiO_2 composites with (a) 0.25, (b) 0.50, (c) 2, and (d) 5 wt % gold initial content, as prepared by route III.

for the structure collapse in route I was most likely due to the breakdown of the agarose gel structure in the acidic gold precursor solution. In route III, hydrolysis of the titania precursor occurred during the template infiltration step because of the presence of the hydrated gold salt. This resulted in thinner layers of titania on the template, with these thin layers unable to support the porous structure after calcination. For route IV, higher concentrations of the gold salt decreased the pH of the hydrolysis solution, thereby altering the sol−gel reaction rates, and hence influencing the final structure.

Characterization of Au/Agarose Gel and Au/TiO_2 Composites. The morphology of the agarose gel, gold nanoparticle/agarose gel, and Au/TiO_2 composite was observed by SEM. Both the gold nanoparticle/agarose gel hybrids for the template of route I and the pure agarose gel for the template of other routes have abundant pores and consistent structures throughout the samples when the gold loading remained below 0.10 wt %. The average pore diameter of the 2 wt % agarose gel or Au/agarose template, as determined from the SEM images, was 110 nm.[37] When the initial gold content was increased to 0.25 wt %, the pore structure of the Au/agarose hybrid deteriorated gradually, possibly from the acidic gold precursor. After heat treatment (450 °C, 10 h), shrinkage of the final Au/TiO_2 nanocomposite to approximately 60% (by volume) of the original wet gold nanoparticle/agarose hybrid was observed, resulting in a corresponding decrease in pore size. However, the porous nature was kept intact during the synthesis, producing highly porous inorganic materials; see Figure 1a−c for route III. For higher concentrations of gold, such as 5 wt % gold initial concentration, the net structure shrank significantly (Figure 1d). The pore structure and pore size did not vary dramatically for similar gold contents (for example, 1 wt %) from routes III to V (Figure 2).

TGA (not shown) was conducted to monitor the mass loss of the samples during heating from room temperature to 800 °C. An overall mass loss of 29 ± 2% for route I, 23 ± 2% for route III, and 24 ± 2% for route IV was observed. At 100 °C, the major mass loss occurred with 20 ± 2, 14 ± 2, and 14 ± 2% losses for routes I, III, and IV, respectively, which resulted from the removal of adsorbed water. The mass loss of 6 ± 2% for all routes occurring around 240 °C was due to the removal of the agarose. No obvious mass loss occurred when heating the samples above 450 °C, suggesting the total removal of the organic species. Differential thermal analysis further indicated that the amorphous titania was crystallized to the anatase phase at ∼420 °C, evidenced by an exothermal peak. Hence, the final calcination conditions were chosen to be 450 °C for 10 h to ensure total removal of the agarose gel template and to crystallize the titania to the anatase phase.

After the calcination treatment, gold nanoparticles were dispersed through the porous oxide structures, as indicated by the uniform sample color. UV−vis diffuse reflectance spectra of the calcined samples showed strong absorbance (corresponding to a marked decrease of reflectance) in the visible wavelength at around 580 nm due to the plasmon resonance of gold, indicating the presence of the gold

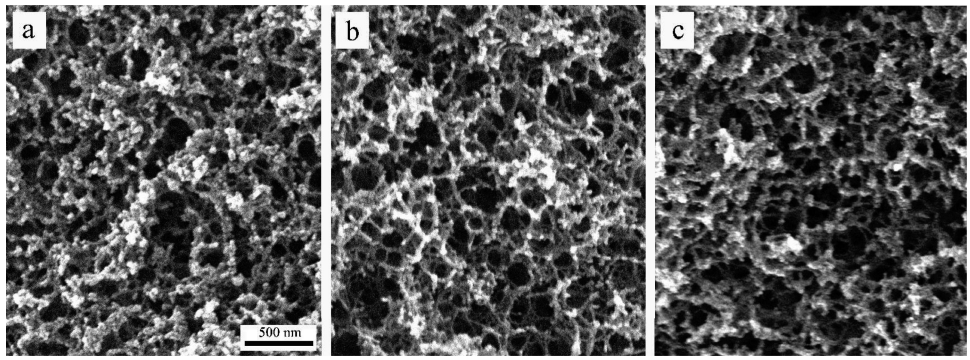

Figure 2. SEM images (all at the same scale) of the Au/TiO_2 composites with 1 wt % gold initial content synthesized by routes (a) III, (b) IV, and (c) V.

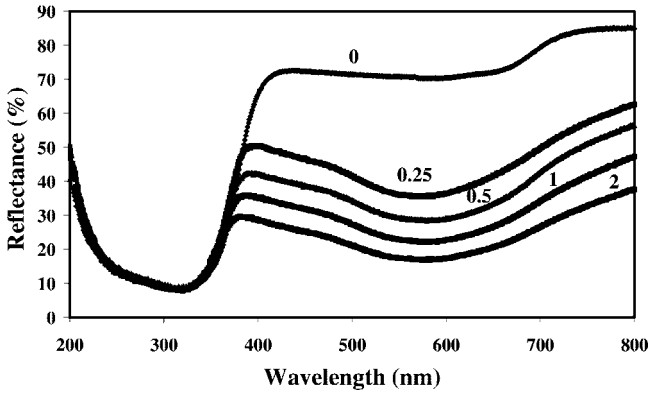

Figure 3. UV−vis diffuse reflectance of the Au/TiO_2 composites synthesized by route V with 0−2 wt % gold initial content.

particles embedded in the TiO_2 matrix. The intensity of the maximum absorbance increased steadily with initial gold concentration in the solution of 0−2 wt % (see Figure 3 for route V). The absorbance intensity increased from route III to route IV to route V for the same initial gold concentration of 1 wt %, which suggested an increased efficiency of gold incorporation.

To investigate the size and distribution of the gold nanoparticles in the final composites, the samples were ultramicrotomed to a thickness of 90 nm and examined under TEM. All samples had abundant pores in the structure (as indicated by the bright areas in the TEM images; Figure 4a). In bright field imaging, strong diffraction contrast from crystalline TiO_2 and high mass thickness because of overlapping TiO_2 in the pore walls made the gold nanoparticles difficult to distinguish from the TiO_2 particles. Plasmon imaging at an energy loss of 20 eV with an energy window of 5 eV was demonstrated to be an effective way to locate the gold particles in this situation.[41] The identification of the gold particles was also confirmed by energy-dispersive X-ray spectroscopy of individual particles.

During sample analysis, plasmon imaging was applied to survey the specimen rapidly to locate the gold particles and then conventional bright field TEM imaging was used to study the structure of the gold particles (Figure 4b−d). For route V, the gold particle size decreased significantly with increasing initial gold concentration in the synthesis solution (Figure 5 and Table 1) to 2.0 wt % gold. However, increasing the gold content to 4 wt % resulted in gold particles with a diameter of 32 ± 10 nm, and some small gold particles were observed. For similar initial gold contents, such as 1 wt %, routes III and IV showed a particle diameter of 35 ± 10 and 25 ± 10 nm, respectively (Figure 4c, d).

Gas sorption analysis was conducted on the agarose gel, agarose/amorphous titania, and porous anatase titania samples, resulting in surface areas of 260.1, 342.0, and 56.3 $m^2\ g^{-1}$, respectively. The amorphous TiO_2 on the surface of agarose gel increased the surface area substantially. From the gas sorption data, the macropore size for the anatase network was 70−80 nm in diameter, a slight decrease from the 80−90 nm pore size in the agarose gel. Mesopores with a diameter of 7−9 nm observed in the final composites most likely resulted from interparticle spacing. Overall, the gold nanoparticle/TiO_2 composites had similar surface areas when compared with that of the agarose templated TiO_2 control (route I: 46.3−56.5 $m^2\ g^{-1}$; route III: 48.6−58.4 $m^2\ g^{-1}$; route IV: 34.6−56.7 $m^2\ g^{-1}$; route V: 48.4−56.0 $m^2\ g^{-1}$), suggesting little influence of the incorporated gold nanoparticles on crystallization of the titania anatase (surface area is inversely proportional to crystal size).

The crystal phase of the materials was obtained from wide-angle powder XRD. All the calcined samples (with or without gold incorporation) were well-crystallized in the anatase phase (see Figure 6 as an example from the route IV samples and Figure 7 for the samples with 2 wt % gold initial content prepared from route III to V). The anatase crystal size of all samples was calculated from the (111) peak at $2\theta = 25.32°$ based on the Scherrer equation[42] and found to be 16 ± 0, 16 ± 2, 15 ± 2, 14 ± 2, and 16 ± 0 nm for control, routes I, III, IV, and V, respectively. Gold diffraction peaks were not observed in the XRD spectra for route I because of the low content of gold in the composites, which was below the detection limit of the XRD instrument.[37] However, gold peaks were detected at 1 wt % of initial gold concentrations for route III, 0.25 wt % for route IV, and 4 wt % for route V. The intensity of the gold peak increased steadily with increasing gold concentration from 0−5 wt %; see gold peak (200) in Figure 6. The gold crystal size was calculated from the diffraction peak (222) at $2\theta = 64.00°$ when sufficient intensity was observed. The most intense diffraction peak (111) was not chosen because of overlap with the (112) titania peak. Overall, the gold crystal size decreased from

(41) Mitchell, D. R. G.; Wang, X.; Caruso, R. A. *Micron* **2007**, *39*, 344.

(42) Cullity, B. D. *Elements of X-ray Diffraction*, 2nd ed.; Addison-Wesley: Reading, MA, 1978.

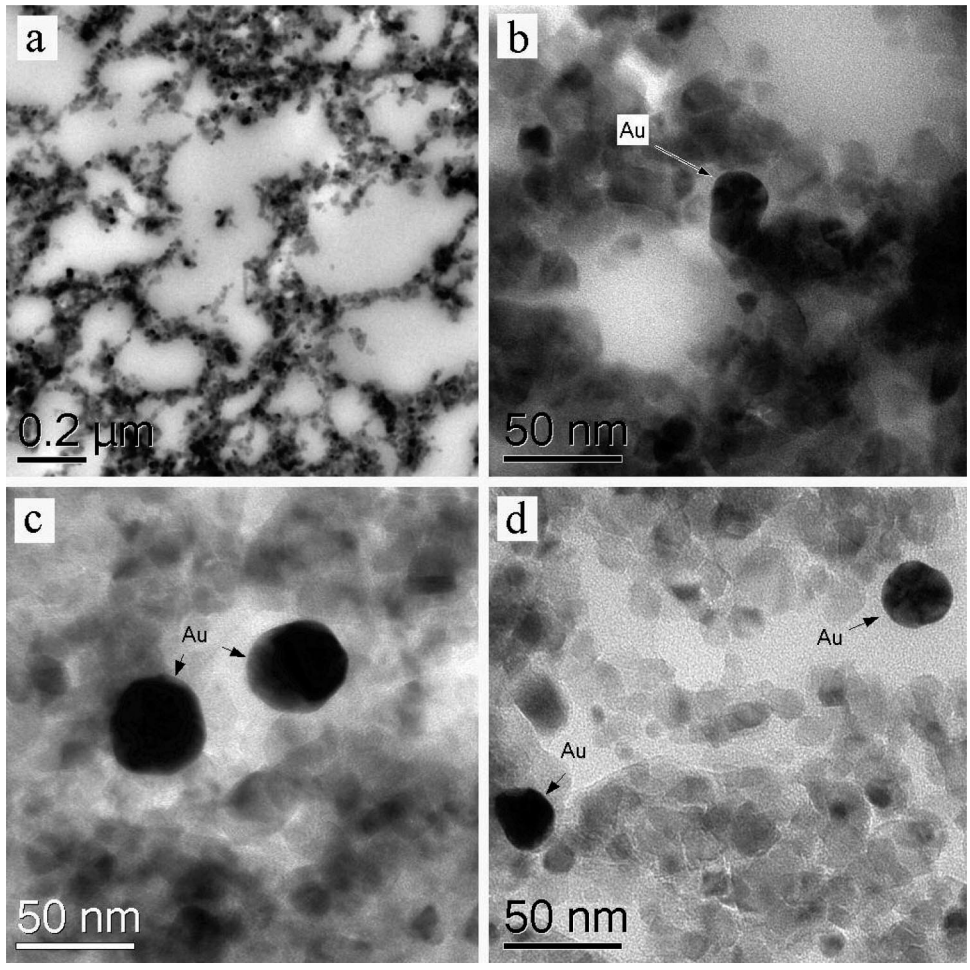

Figure 4. TEM images of the Au/TiO_2 composites from synthesis: (a) route I with 0.10 wt % initial gold content, (b) higher magnification of route I, 0.10 wt % initial gold content, (c) route III with 1 wt % initial gold content, and (d) route IV with 1 wt % initial gold content.

route III (range from 24−27 nm corresponding to 1.0−5.0 wt % of initial gold) to route IV (range from 17−23 nm corresponding to 1.0−5.0 wt % of initial gold) to route V (18 nm corresponding to 4 wt % of initial gold) under the same initial gold content. The gold crystal size generally increased with increasing gold content using the same synthesis route. It should be noted that the gold crystal size determined from XRD was smaller than the particle diameter from the TEM observation because of agglomeration of crystals to form particles. In route V, the gold peak was only observed in samples with high gold concentration because of the gold particle diameter remaining small ($\leq$10 nm) and being uniformly distributed throughout the TiO_2 porous structures (from TEM observation).

SIMS was utilized to examine the distribution of the gold nanoparticles within the porous titanium dioxide matrix. A peak at 65 amu ($^{49}Ti^{16}O$) was chosen to represent TiO_2 because of fewer mass interferences at this channel in the spectrometer (the relative standard deviation was less than 8%). The yield of gold (^{197}Au) secondary ions was observed to be relatively uniformly distributed with depth into the porous titania network. This was evidenced through the relatively stable ^{197}Au and $^{49}Ti^{16}O$ counts over 5 μm in depth (see Figure 8 as an example). The gold yield observed between the different materials steadily increased, corresponding to the increasing initial gold concentration in the synthesis solutions from 0.25−4 wt % for route V. To compare the gold incorporation efficiency across the synthesis routes, the same initial gold amount of 1 wt % was studied. It was demonstrated that route V gave the highest quantity of gold in the final product (1.65 count/count (c/c)) as compared with routes IV (1.01 c/c) and III (0.69 c/c) (Figure 8). In addition, the gold distribution became more uniform with increasing incorporation efficiency. The gold distribution fluctuated slightly in both routes III and IV because of the larger gold particle size generated in these routes.

ICP analysis was used to quantitatively determine the gold content in the final gold nanoparticle/TiO_2 composites (Figure 9, relative standard deviation <2%). The gold content increased steadily with increasing gold concentration in the synthesis solution, with approximately half of the initial gold quantity incorporated into the final materials for route I. The total gold content was limited in route I by the gel stability in the presence of the gold salt solution. Higher gold contents could be obtained for synthesis routes III−V with gold incorporation efficiencies around 10−30, 70, and 90% of the initial concentration for routes III, IV, and V, respectively. Overall, the higher the gold concentration during synthesis, the more gold was incorporated within the final composite. However, for route III, when the gold concentration during synthesis was greater than 1 wt %, the gold content in the final composite decreased. ICP results further confirmed

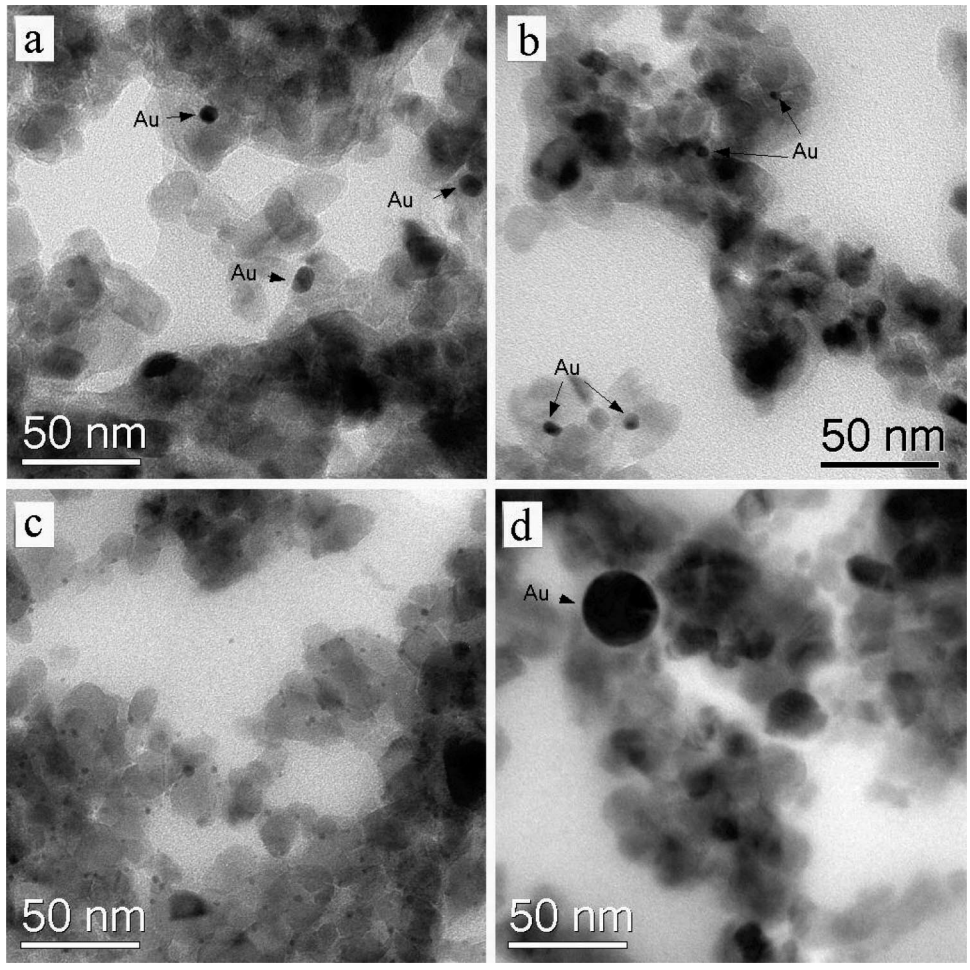

Figure 5. TEM images of the Au/TiO_2 composites from route V with (a) 0.50, (b) 1.0, (c) 2, and (d) 4 wt % gold initial content.

Table 1. Gold Crystal and Particle Diameter (in Nanometers) Determined by XRD and TEM for the Au/TiO_2 Composites Synthesized from Routes III, IV, and V

	route III		route IV		route V	
Au (wt %)[a]	XRD	TEM	XRD	TEM	XRD	TEM
0.25	nd[b]		nd		nd	20 ± 12
0.5	nd		nd		nd	8 ± 3
1	24	35 ± 10	17	25 ± 10	nd	6 ± 2
1.5	24		18			
2	25		17		nd	2 ± 1
2.5	27		19			
4					18	32 ± 10
5	nd		23			

[a] wt %: The initial gold content in synthesis. [b] nd: Insufficient intensity or no gold peak detected in the XRD data.

SIMS analysis that the gold incorporation efficiency for the four routes was route V > route IV > route I > route III.

Photocatalytic Activity of the Au/TiO_2 Composites. Various reactions have been used to examine the photocatalytic activities of Au/TiO_2 based catalysts. Azo-dyes (e.g., methylene blue and methyl orange) and industrial impurities (such as phenol, thiocyanate anion, or bisphenol A) are often applied as the probe molecules.[43–47] It was demonstrated that

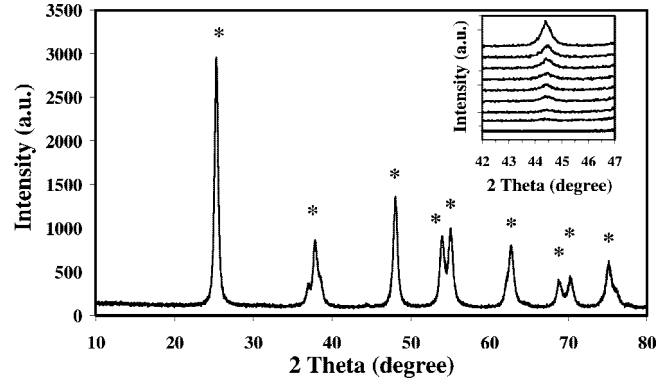

Figure 6. X-ray diffraction patterns of the Au/TiO_2 composites synthesized by route IV with 0.25 wt % initial gold content. Inset shows (200) peak of gold from bottom to top with increasing gold content of 0, 0.25, 0.5, 1, 1.25, 1.5, 2, 2.5 and 5 wt % (* anatase peak).

Au/TiO_2 showed enhanced photocatalytic activity over TiO_2 under either UV or visible light illumination. The optimum gold loading in the Au/TiO_2 photocatalysts ranges from ~0.5 to 2 wt % depending on the different synthesis approaches.[43–47]

In our study for photocatalytic activity, methylene blue, an organic dye, was chosen as the probe molecule. During the photocatalytic reaction, the concentration of methylene

(43) Arabatzis, I. M.; Stergiopoulos, T.; Andreeva, D.; Kitova, S.; Neophytides, S. G.; Falaras, P. *J. Catal.* **2003**, *220*, 127.
(44) Li, F. B.; Li, X. Z. *Appl. Catal., A* **2002**, *228*, 15.
(45) Sonawane, R. S.; Dongare, M. K. *J. Mol. Catal. A: Chem.* **2006**, *243*, 68.
(46) Li, X. Z.; He, C.; Graham, N.; Xiong, Y. *J. Appl. Electrochem.* **2005**, *35*, 741.

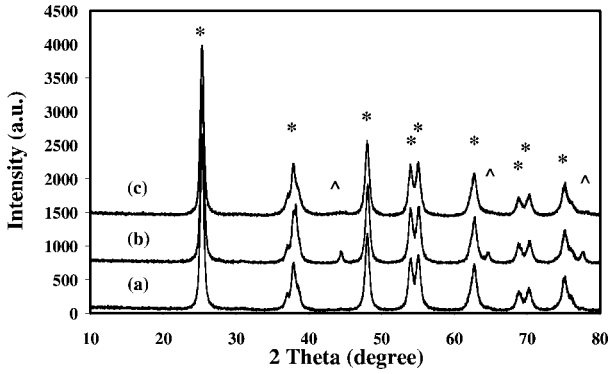

Figure 7. XRD patterns of the Au/TiO$_2$ composites with 2 wt % gold initial content synthesized by routes (a) III, (b) IV, and (c) V (* anatase peak, ^ gold peak).

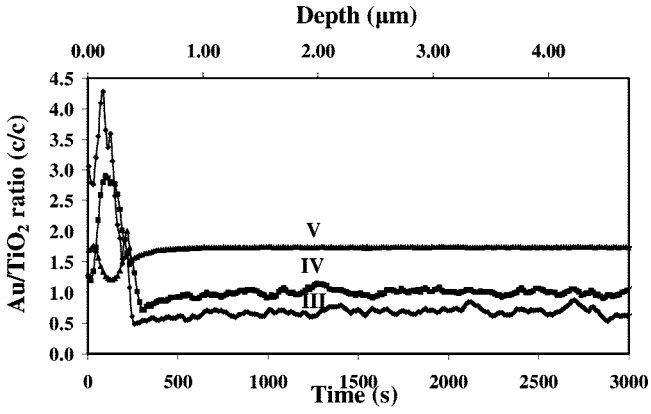

Figure 8. SIMS analysis of the Au/TiO$_2$ composites as a function of depth (top *x*-axis) and sputter time (bottom *x*-axis) prepared by routes III, IV, and V with 1 wt % gold initial content.

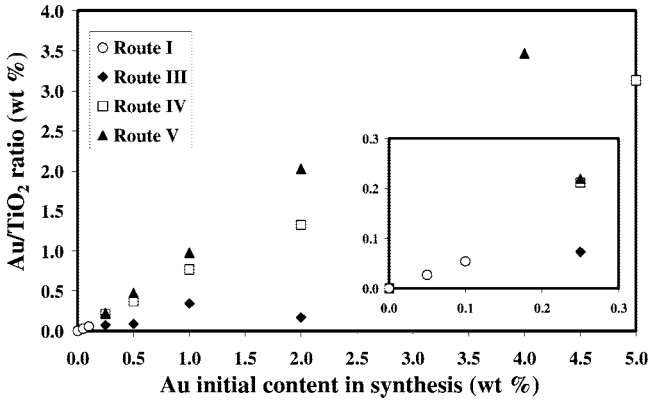

Figure 9. Au/TiO$_2$ ratio (wt %) determined by ICP in the composites prepared from routes I, III, IV, and V. Inset shows an enlargement of the low gold content with the same axis titles as the main figure.

blue was monitored every 10 min. The photocatalytic activity, given as a percentage, refers to the difference in methylene blue concentration immediately before irradiation, $C(0)$, and after 60 min UV light irradiation, $C(60)$, divided by the concentration before irradiation (i.e., $100*[C(0) - C(60)]/C(0)$). The photocatalytic reaction was repeated with the control sample six times, giving reproducible data (relative standard deviation within 3%). There was no noticeable change in photocatalytic activity for increasing

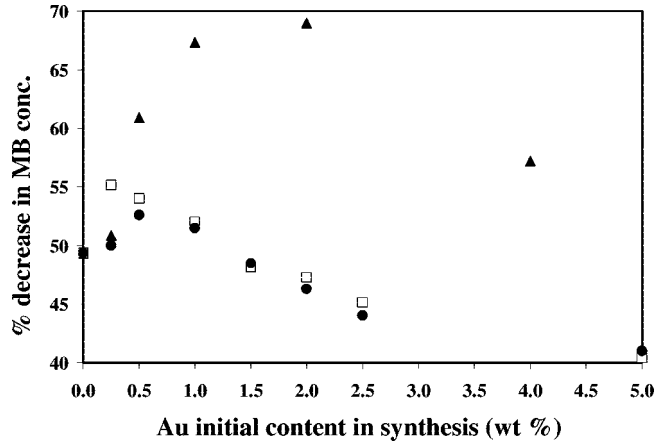

Figure 10. Photocatalytic activity of the Au/TiO$_2$ composites synthesized by route III (□), IV (●), and V (▲) plotted as the difference in methylene blue concentration (as a percentage of original concentration) after 60 min of UV light irradiation.

gold content in the samples from route I. The photocatalytic activity of Au/TiO$_2$ materials from routes III and IV fluctuated around the control sample (TiO$_2$), and there was only slight enhancement at low gold content (Figure 10). For route III, 0.25 wt % gold sample gave the best photocatalytic activity (55 vs 49% for the control), further increasing gold content to 5 wt % decreased the activity to 40%. For route IV, the optimum activity was 53% for the 0.5 wt % gold sample. However, the photocatalytic activity of route V increased significantly with increased gold content. The optimum photocatalytic activity was 69% for the 2 wt % initial gold concentration sample, which was a 40% enhancement compared with that of the control (Figure 10).

This study confirmed that the size of gold particle in the final composite and also the total gold content, as determined by the synthesis route, influence the photocatalytic activity. If the gold particle diameter is below 10 nm, the gold content plays the major role in altering the photocatalytic activity. No clear trend can be found between the photocatalytic activity and surface area of the materials in the current system. An insignificant change in photocatalytic activity was observed for route I. We propose that this is due to both the large gold particle diameter (>10 nm) and low loading quantities (<0.05 wt %). For routes III and IV, the gold particle diameter was considerably larger than 10 nm (such as 35 nm for route III and 25 nm for route IV with gold initial content of 1 wt %). Hence, the large gold nanoparticle may serve as an electron−hole recombination center rather than decreasing such recombinations.[48] However, in route V, most of the gold particles were smaller than 10 nm based on TEM observation. Therefore, the photocatalytic activity of all the materials from route V showed improvement, with the best material having a gold content of 2.0 wt % and the smallest gold particle diameter (2 ± 1 nm).

In summary, a number of synthesis routes have been studied to fabricate porous gold nanoparticle/TiO$_2$ nanocomposites using a templating technique. The morphology, pore diameter, gold and anatase crystal size, and gold content and distribution in the materials were analyzed. The most

(47) Kamat, P. V. *Pure Appl. Chem.* **2002**, *74*, 1693.

(48) Li, X. Z.; Li, F. B. *Environ. Sci. Technol.* **2001**, *35*, 2381.

effective gold incorporation using these synthesis methods was by deposition of gold on a prefabricated porous TiO_2 (route V), followed by introduction of the gold salt in the hydrolysis solution (route IV), the addition of gold salt during template formation (route I), and last mixing the gold salt with the titania precursor for the infiltration step (route III). Route V produced the smallest gold nanoparticles when comparing samples prepared with the same initial gold concentrations. The photocatalytic activity was investigated, where the gold particle diameter and total content in the sample, determined by the synthesis route, could be correlated to the activity. The sample as prepared by route V with the highest photocatalytic activity had gold nanoparticles of 2 ± 1 nm in diameter and 2.0 wt % gold content in the final product. The versatility of this method allows for the preparation of other noble metals on similar agarose or metal oxide supports.

Acknowledgment. This work was supported by funding from the Australian Research Council and awards (AINGRA07026 and AINGRA06027) from the Australian Institute of Nuclear Science and Engineering. R.A.C. acknowledges the ARC for an Australian Research Fellowship. Dr Simon Crawford is thanked for ultramicrotoming samples in preparation for TEM, and Fuzhi Huang is appreciated for running the diffuse UV−vis spectroscopy.

CM703509F